Gap resonances analyzed by a domain-decomposition method

Trygve Kristiansen[1,2] **and Odd M. Faltinsen**[1]

[1]Department of Marine Technology and Center for Ships and Ocean Structures,
Norwegian University of Science and Technology, Trondheim, Norway

[2] MARINTEK, Trondheim, Norway

Corresponding author: trygve.kristiansen@ntnu.no

Introduction. Gap resonance problems have been addressed in recent years both by industry (Bunnik et al. (2009)) and in more academic works (Kristiansen and Faltinsen (2009), Molin et al. (2009), Lu et al. (2010), Sun et al. (2010)). Examples are ship-by-ship operations, moonpools and LNG carriers alongside terminals. Traditional panel methods may greatly overestimate the fluid and body motions around the gap resonance frequencies. The reason is that linear damping from radiated waves may be small compared to the damping provided by flow separation e.g. at bilge keels.

Our objective is to develop a physically based method which is fast relative to solving the complete problem with a Naviér-Stokes solver (CFD), and comparable in time with potential flow solvers.

We are at the moment developing a time-domain numerical wavetank based on domain-decomposition. The main part of the wavetank has linearized potential flow, but we incorporate the effect of flow separation using CFD in a *submerged domain* around the body. The thought is that potential theory is best at propagating waves, while the CFD incorporates flow separation e.g. at bilge keels.

The present domain-decomposition method is inspired by the study in Kristiansen and Faltinsen (2008); gap resonance problems are well modelled by linearized free-surface conditions, as long as flow separation is included.

The present work is two-dimensional, but the method is directly applicable for a three-dimensional implementation.

Theory. Consider a closed two-dimensional wavetank filled with incompressible water as in Figure 1. We assume that in most of the wavetank the water is inviscid, but viscous near the ship bilges. The basic equations are the Bernoulli equation in the inviscid domain Ω_0 and the Naviér-Stokes equations in the viscous domain Ω_v,

$$\frac{\partial \varphi}{\partial t} + 0.5\nabla\varphi\cdot\nabla\varphi = -\frac{1}{\rho}p - gz \quad \text{in } \Omega_0, \tag{1}$$

$$\frac{\partial \mathbf{u}}{\partial t} + \mathbf{u}\cdot\nabla\mathbf{u} = -\frac{1}{\rho}\nabla p - g\hat{\mathbf{k}} + \nu\nabla^2\,\mathbf{u} \quad \text{in } \Omega_v, \tag{2}$$

along with the requirement of continuity of mass,

$$\nabla\cdot\mathbf{u} \;=\; 0. \tag{3}$$

Here, $\mathbf{u} = (u, w)$ is the fluid velocity, φ is the velocity potential, g is the acceleration of gravity, $\hat{\mathbf{k}}$ is the unit vector in the positive $z-$direction, ρ is the water density and ν is the kinematic viscosity. In the inviscid domain $\mathbf{u} = \nabla\varphi$, while in the viscous domain, $\mathbf{u}$ is found from (2). The velocity potential satisfies the Laplace equation $\nabla^2\varphi = 0$.

We require that (a) the normal velocity and (b) the pressure are continuous along the boundary that separates the two domains.

We further assume that the fluid flow everywhere away from sharp corners is well described by linear theory, so we neglect the nonlinear term in (1). We introduce the acceleration potential $\psi = \frac{\partial\varphi}{\partial t}$ which also satisfies the Laplace equation. In the inviscid domain we then have the free-surface problem described by

$$\begin{aligned}
\frac{\partial\varphi}{\partial t} &= \psi \qquad \text{in } \Omega_0,\\
\frac{\partial\zeta}{\partial t} &= \frac{\partial\varphi}{\partial z} \qquad \text{on } z = 0,\\
\psi &= -g\zeta \qquad \text{on } z = 0,\\
\frac{\partial\psi}{\partial n} &= \dot{U}_w \qquad \text{on } S_{B0},\\
\nabla^2\psi &= 0 \qquad \text{in } \Omega_0,
\end{aligned} \tag{4}$$

where $\zeta(x,t)$ is the free surface elevation, $\dot{U}_w$ is the local body acceleration and S_{B0} is the mean body position. For convenience we denote $\tilde{p} = -p/\rho - gz$.

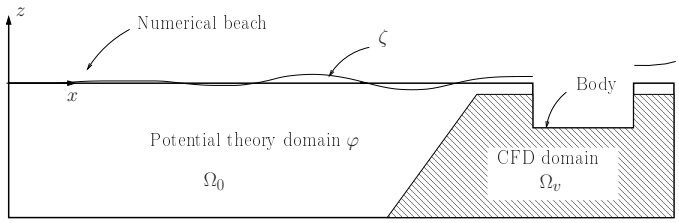

Figure 1: Sketch of numerical wavetank. The computational domain is fixed and denoted $\Omega_0 + \Omega_v$.

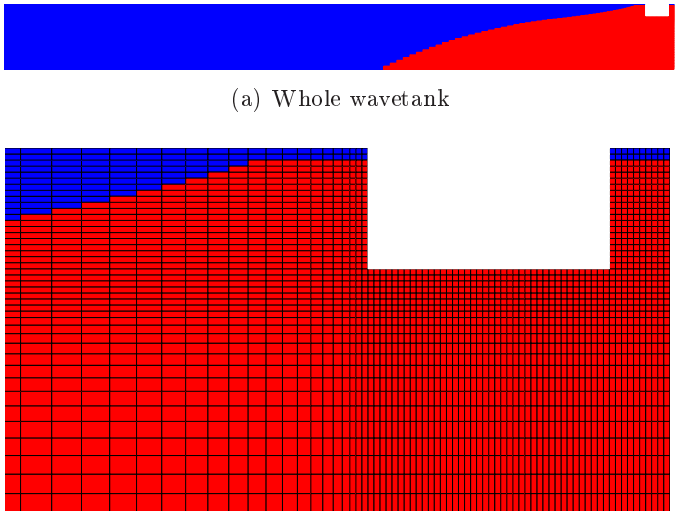

(a) Whole wavetank

(b) Zoom around structure

Figure 2: The numerical wavetank with two domains. Blue: Inviscid domain Ω_0. Red: Viscous domain Ω_v.

Now (1) and (2) are

$$\psi = \tilde{p}, \tag{5}$$

$$\frac{\partial \mathbf{u}}{\partial t} + \mathbf{u} \cdot \nabla \mathbf{u} = \nabla \tilde{p} + \nu \nabla^2 \mathbf{u}. \tag{6}$$

There are two discrepancies in what we model in the two domains: One is that the inviscid method does not handle vorticity. From our experience so far, it seems that we may handle this in practice by having the Naviér-Stokes domain large enough. The cpu time is not sensitive to the size of the CFD domain. The second discrepancy is that the linearized potential theory does not take into account nonlinearities, while the Naviér-Stokes solver does via the term $\mathbf{u}\cdot\nabla\mathbf{u}$ which is essential due to advection of vorticity. If the free-surface flow becomes "nonlinear", the two solvers do not really solve for the same physics, and we expect problems. One example is in a closed sloshing tank, another example is in steep waves. However, in gap resonance problems the flow is well described by linearized free-surface conditions; the two different solvers solve the same physics, and the present domain-decomposition method becomes useful.

Numerical implementation. We use a fourth order explicit Runge-Kutta method to time-step the solution φ and ψ according to (4) in the inviscid domain, and $\mathbf{u}$ in the viscous domain. We use one standard way to solve the Naviér-Stokes equations (2) and (3) numerically, called the *fractional step method*. In principle, going from time-step n to $n+1$: (A) advection, (B) apply viscosity, and (C) solve Poisson equation and update to a divergence free velocity field $\mathbf{u}^{n+1}$. One may say that the essential roles are for step (B) to create vorticity along walls, and for step (A) to advect this vorticity into the main part of the fluid. Step (C) is mathematically stated as

$$\nabla^2 \tilde{p} = \nabla \cdot \mathbf{u}^{\star\star}/\Delta t, \quad \mathbf{u}^{n+1} = \mathbf{u}^{\star\star} + \Delta t\, \nabla \tilde{p}, \tag{7}$$

where $\mathbf{u}^{\star\star}$ is the artificial velocity field after steps (A) and (B), which is not divergence free, whereas $\mathbf{u}^{n+1}$ is divergence free.

If we now look at (5) we see that we may treat $\tilde{p}$ and ψ as the same variable. Next compare the last equation in (4), and equation (7) and note that $\tilde{p}$ and ψ are acted upon by the same operator; the Laplacian ∇^2. If we choose the same numerical method to solve for $\tilde{p}$ and ψ, we may use the same discretization method for both and we obtain one single system of equations $Ax = b$ for the whole wavetank. This ensures that *both matching conditions are satisfied* without any further exchange of information between the two domains. In this way we avoid having an overlapping region, and we avoid any back-and-forth communication. There is a sharp interface between the two domains. To the authors' knowledge, this method to couple potential theory with a Naviér-Stokes solver is new.

We chose to use the Finite Volume Method (FVM) in both domains. We discretize the whole wavetank by rectangles (see Figure 2) and assume all variables to be constant over each rectangle face. The method for advection is simply upwinding. This is diffusive, but sufficient for our purpose, where the shed vorticity is important only for about half a wave period. We call the present code the *dd-code* hereafter.

Results. We present three studies; two with compar-

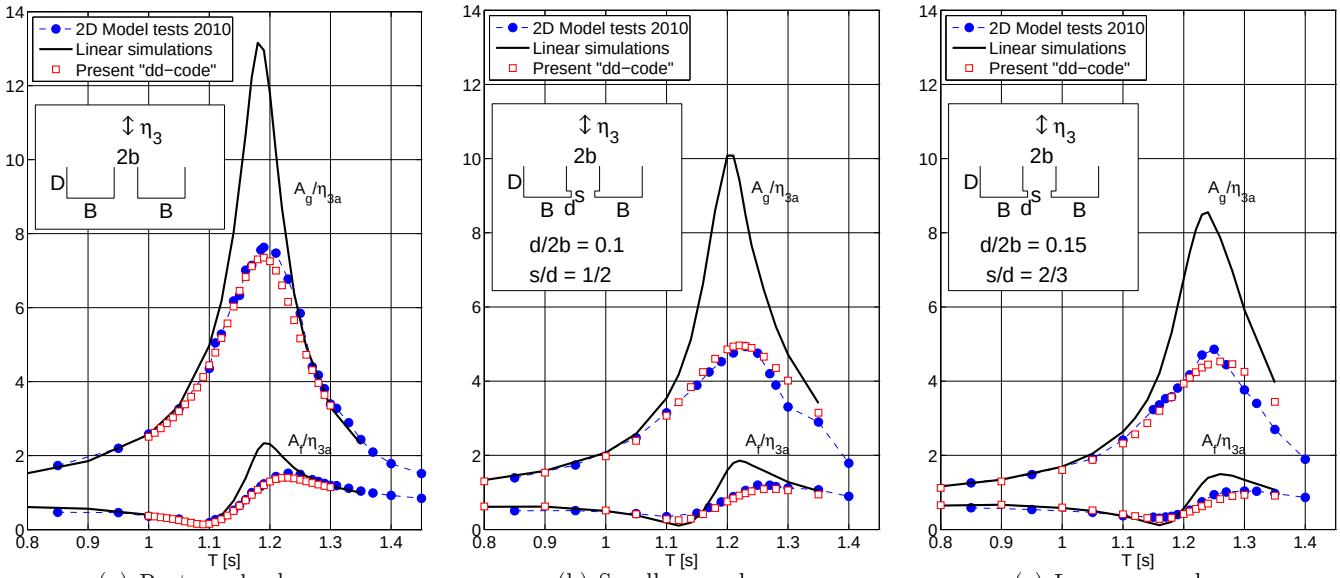

(a) Rectangular boxes (b) Small appendages (c) Large appendages

Figure 3: Forced heave of two rigidly connected boxes with no (left plot), or different sized, appendages.

ison against experimental data for validation, and one purely numerical.

Study 1: Moonpool. Two rigidly connected boxes are forced to heave. Experiments were carried out at Marintek in January 2010. The results are compared to the present numerical results in Figure 3 (a - c). $B = 0.36$m, $D/B = 0.5$, $b/B = 0.25$, the forced heave amplitude is $\eta_{3a} = 5$mm, and the water depth is $h = 1.03$m. The appendage size s and d are varied between the three plots. A_g is the steady-state amplitude averaged over the gap and A_f is the far-field amplitude. The results called "Linear simulations" are also performed with the present dd-code with advection and diffusion turned off (icfd = 0). This recovers the linear solution.

We see that linear theory overpredicts by about 75%, while the simulations including flow separation (called "Present dd-code") compare well with the model tests. This indicates that the present dd-method is appropriate to use in analyzing gap resonance problems.

The appendages have two effects: (1) They cover part of the moonpool inlet (the small and large appendages cover 20% and 30% of the moonpool inlet, respectively), and (2) they cause stronger vorticity than a square corner as the flow "sees" nearly a flat plate.

Steady-state was typically achieved after about 15 - 20 periods. Each marker in the figures is the average of the amplitude over the last 10 periods in a 30 period long run. The grid is nearly uniform around the body as shown in Figure 2 and stretched both in the vertical and horizontal directions away from the ship. We tried different resolutions: 4, 6, 10 and 20 grid cells across the gap. All gave practially the same results. This means the gap resonance problem is not sensitive to gridding, at least for this simple body geometry.

Only half the physical domain was modelled due to symmetry across the moonpool mid-line. For the whole wavetank we had $n_x = 150$ and $n_z = 54$ (approximately $N = 7300$ unknowns). The number of time-steps per period was 80. The cpu-time was remarkably low; running 30 periods (2400 time-steps) took only 73 seconds on a single 2.4GHz cpu.

Study 2: A ship section by a vertical wall. A rectangular ship section was moored and free to sway, heave and roll in incoming waves. The set-up is described in Kristiansen and Faltinsen (2009). $B = 0.4$m, $B/D = 4$ and the distance to the wall was $b/B = 0.2$. The results are presented in Figure 4. The agreement is good between the dd-code and the experiments. $n_x = 168$, $n_z = 30$ and $N = 4640$. Running 50 periods (4000 time-steps) took 140 seconds. Linear theory overpredicts by about 300%. In the experiments, there was a slight mean drift of about $0.03b$

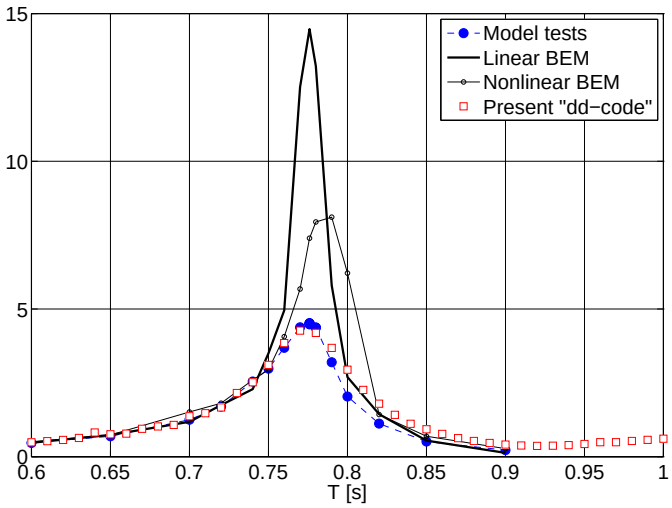

Figure 4: A_g/A. A rectangular box by a vertical wall in incoming waves $B = 0.4$m, $B/D = 4$ and $b/B = 0.2$. A is incoming wave amplitude.

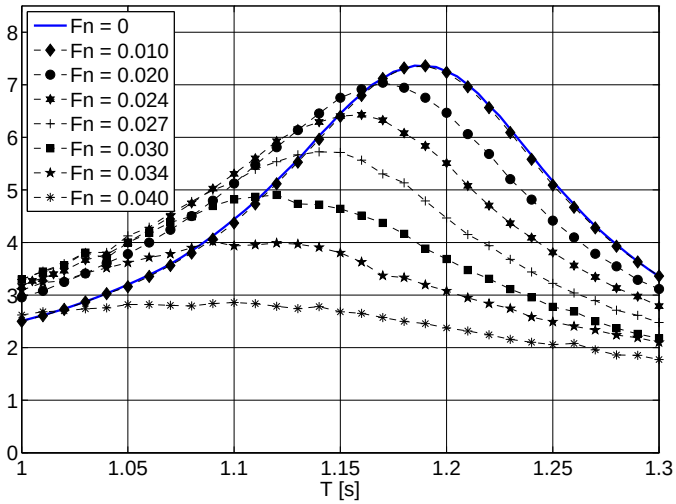

Figure 5: A_g/η_{3a}. Forced heave of moonpool in a current U. Simulations by the present dd-code.

away from the wall at resonance. This is not incorporated in the present dd-code (linearized boundary conditions). It seems that the drift is not important in the present situation, but we can not say so in general. The nonlinear BEM results seemingly gives an improved result, but we believe this is due to the fact that the system drifted of resonance; the mean drift around resonance was about $0.1b - 0.15b$.

Study 3: Moonpool in current. This is like Study 1, except there is also a current from left to right. The numerical domain is twice as long as that used in Study 1 (see Figure 2); both ship sections are modelled and the tank extends also to the right of the sections. The results are presented in Figure 5. $n_x = 285$, $n_z = 24$ and $N = 6840$. Running 50 periods (8000 time-steps) took about 5 minutes. The Froude number is $Fn = U/\sqrt{2g(B+b)}$. The main result is that there is no effect of the current at $Fn = 0.01$, a small effect when doubling to $Fn = 0.02$, while a large effect when doubling again to $Fn = 0.04$.

Ongoing and further work. We are presently working on two matters. One is implementing an immersed boundary method with local refinement in order to represent more general body geometries. The other is to add weakly nonlinear free-surface conditions because the gap size may change due to large mean forces from the large piston-mode motion.

We gratefully acknowledge MARINTEK for allowing the use of the moonpool model test data.

References

Bunnik, T., W. Pauw, and A. Voogt (2009). Hydrodynamic analysis for side-by-side offloading. In *Proc. 19th Int. Offshore and Polar Eng. Conf.*

Kristiansen, T. and O. M. Faltinsen (2008). Application of a vortex tracking method to the piston-like behaviour in a semi-entrained vertical gap. *Appl. Ocean Res. 30*, 1–16.

Kristiansen, T. and O. M. Faltinsen (2009). A two-dimensional numerical and experimental study of resonant coupled ship and piston-mode motion. *Appl. Ocean Res. 32*, 158–176.

Lu, L., L. C., B. T., and L. S. (2010). Comparison of potential flow and viscous fluid models in gap resonance. In *25th Int. Workshop on Water Waves and Floating Bodies*.

Molin, B., F. Remy, A. Camhi, and A. Ledoux (2009). Experimental and numerical study of the gap resonances in-between two rectangular barges. In *13th Congr. of Intl. Maritime Ass. of Meditarranean (IMAM)*.

Sun, L., E. T. R., and P. Taylor (2010). First- and second-order analysis of resonant waves between adjacent barges. *J. Fluids and Struct. 26*, 954–978.